NUMERICAL SIMULATION OF DEFLAGRATION-TO-DETONATION TRANSITION

Leonid Kagan and Gregory Sivashinsky

Sackler Faculty of Exact Sciences, School of Mathematical Sciences,

Tel Aviv University, Tel Aviv 69978, Israel

	Deflgartion	Detonation
Speed	subsonic	supersonic
Driving Mechanism	heat flux	heating by shock
Initiation	spark	explosion

.

$$\gamma\Theta_\tau - (\gamma-1)\Pi_\tau = \gamma\epsilon\Theta_{\xi\xi} + \Omega(\Phi,\Theta)$$

$$\Phi_\tau = \epsilon Le^{-1}\Phi_{\xi\xi} - \Omega(\Phi,\Theta)$$

$$\Pi_\tau - \Theta_\tau = \Pi_{\xi\xi}$$

$\Theta = (T-T_u)/(T_b-T_u)$ is the scaled temperature, $\Pi = (P-P_u)/(P_b-P_u)$ the scaled pressure, $\Phi = C/C_u$ the scaled concentration, $\Omega(\Phi,\Theta) \sim C\exp(-E/RT)$ the scaled reaction-rate. ξ, τ are the appropriately scaled spatio-temporal coordinates; $\gamma = c_p/c_v$, Le = Lewis number. $\epsilon = D_{th}/D_{bar}$ is the thermal diffusivity/pressure diffusivity ratio.

$$D_{bar} = Ka_u^2/\gamma\nu$$

where, K = porous bed permeability, ν=kinematic viscosity, a_u=sonic velocity in the unburnt gas.

$$\epsilon \sim 10^{-7} - 10^{-4}$$

(i) the fast wave sustained by the diffusive transfer of pressure (subsonic detonation), and

(ii) the slow wave sustained by the diffusive transfer of heat (deflagration).

In the subsonic detonation regime for the leading order asymptotics the original model (1)-(3) simplifies to

$$\gamma\Theta_\tau - (\gamma-1)\Pi_\tau = \Omega(\Phi,\Theta)$$

$$\Phi_\tau = -\Omega(\Phi,\Theta)$$

$$\Pi_\tau - \Theta_\tau = \Pi_{\xi\xi}$$

This shortened system admits to the traveling wave solution

$$\Phi = \Phi(\xi-\lambda\tau), \Pi = \Pi(\xi-\lambda\tau), \Theta = \Theta(\xi-\lambda\tau).$$

propagating at velocity $\lambda \sim 1$.

In the deflagration regime $\Pi \sim \sqrt{\epsilon}, \xi \sim \sqrt{\epsilon}$ and for the leading order asymptotics the original model, yields

$$\gamma\Theta_\tau = \gamma\epsilon\Theta_{\xi\xi} + \Omega(\Phi,\Theta)$$

$$\Phi_\tau = \epsilon Le^{-1}\Phi_{\xi\xi} - \Omega(\Phi,\Theta)$$

$$\Pi_{\xi\xi} = 0.$$

The system is obviously nothing but a conventional constant-density model for the free-space deflagration;

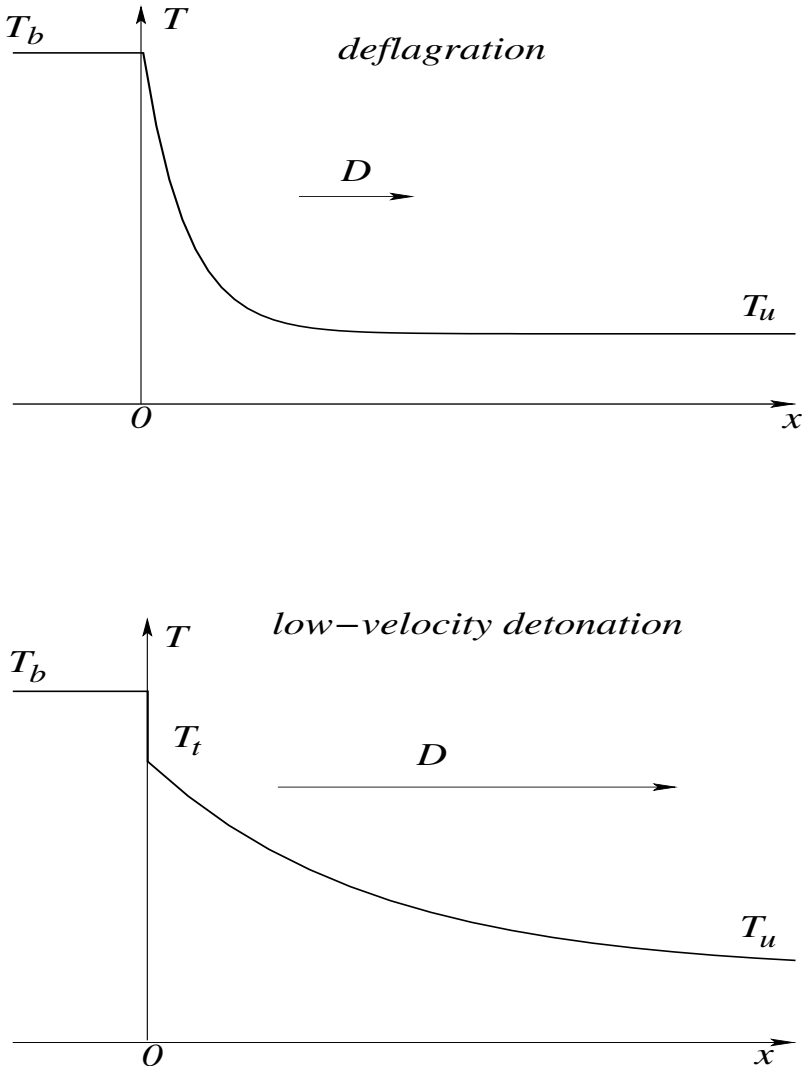

Figure 1: Temperature distribution in the deflagration and detonation waves.

The higher-order approximation for subsonic detonation, i.e. incorporation of the thermal diffusivity effects, does not produce any significant change in the overall dynamical picture. There still exists a steady traveling wave solution with $\lambda \sim \sqrt{\epsilon}$.
For the deflagration the picture is different. Here, the higher order approximation, i.e., accounting for the porous bed resistance, leads to the local elevation of pressure. The pressure, however, does not stabilize at some low level but rather keeps growing as $\Pi \sim \sqrt{\epsilon\tau}$.

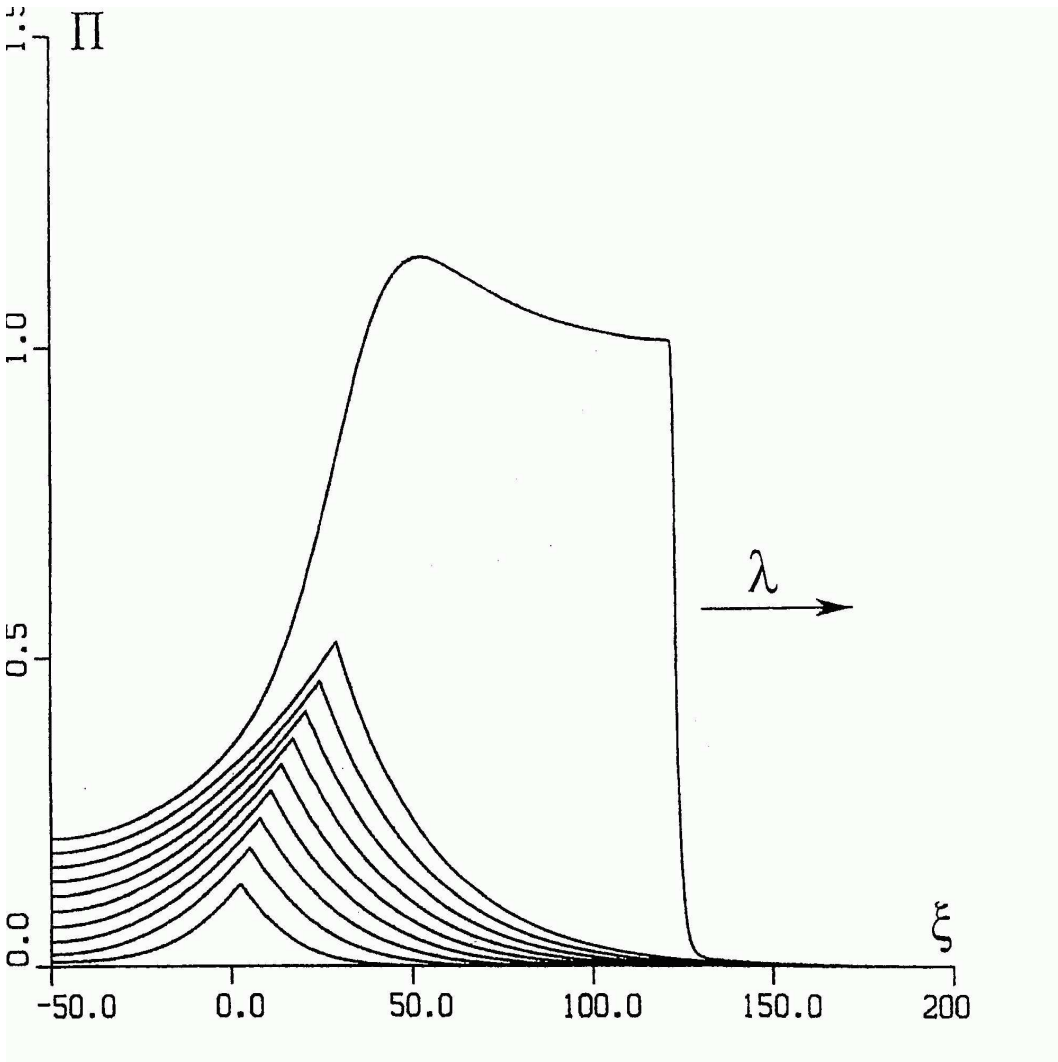

Figure 2: Pressure distribution.

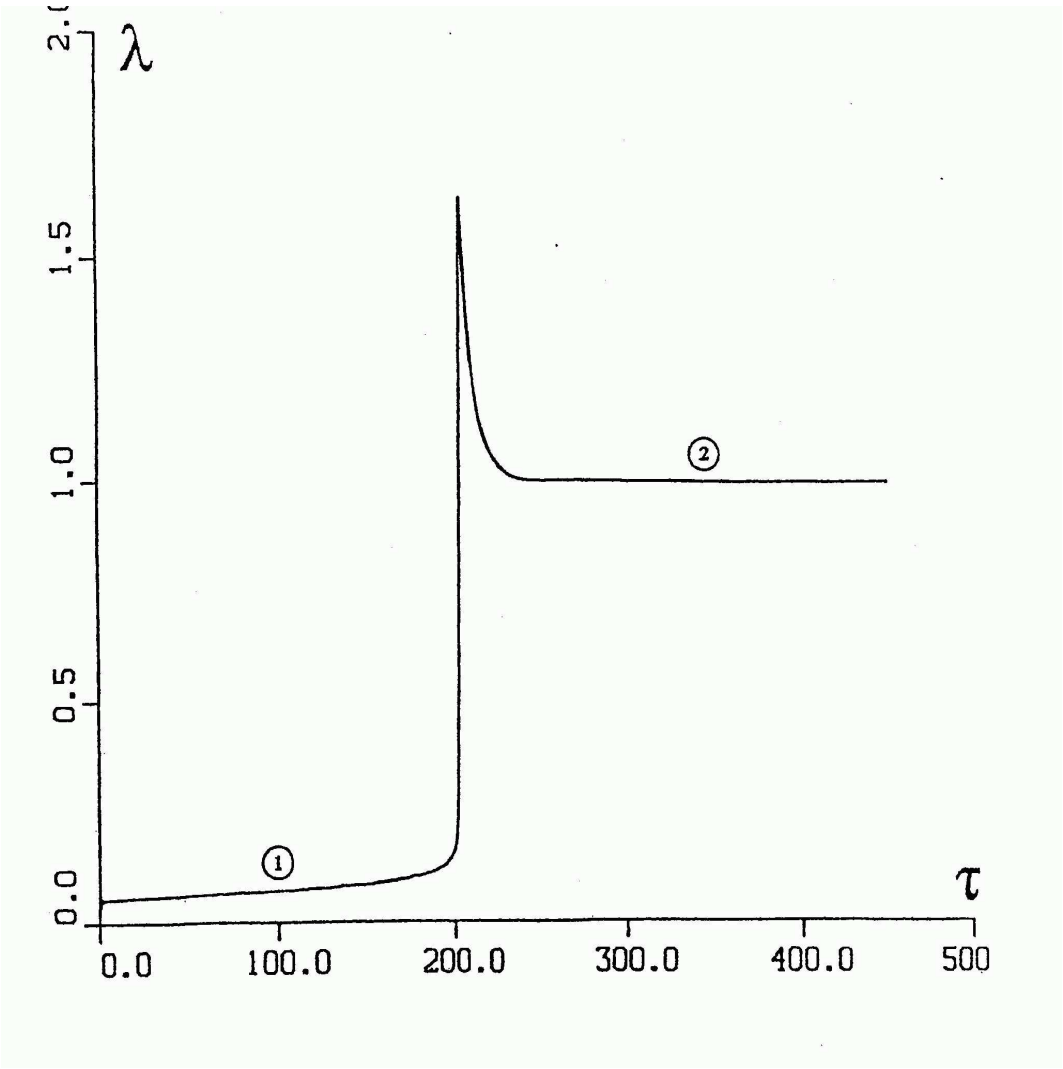

Figure 3: Flame speed.

continuity and state,

$$\frac{\partial \hat{\rho}}{\partial \hat{t}} + \frac{\partial \hat{\rho}\hat{u}}{\partial \hat{x}} + \frac{\partial \hat{\rho}\hat{v}}{\partial \hat{y}} = 0, \qquad \hat{P} = \hat{\rho}\hat{T},$$

momentum,

$$\hat{\rho}\left(\frac{\partial \hat{u}}{\partial \hat{t}} + \hat{u}\frac{\partial \hat{u}}{\partial \hat{x}} + \hat{v}\frac{\partial \hat{u}}{\partial \hat{y}}\right) + \frac{1}{\gamma}\frac{\partial \hat{P}}{\partial \hat{x}} =$$

$$\epsilon Pr\left[2\frac{\partial^2 \hat{u}}{\partial \hat{x}^2} + \frac{\partial}{\partial \hat{y}}\left(\frac{\partial \hat{u}}{\partial \hat{y}} + \frac{\partial \hat{v}}{\partial \hat{x}}\right) - \frac{2}{3}\frac{\partial}{\partial \hat{x}}\left(\frac{\partial \hat{u}}{\partial \hat{x}} + \frac{\partial \hat{v}}{\partial \hat{y}}\right)\right],$$

$$\hat{\rho}\left(\frac{\partial \hat{v}}{\partial \hat{t}} + \hat{u}\frac{\partial \hat{v}}{\partial \hat{x}} + \hat{v}\frac{\partial \hat{v}}{\partial \hat{y}}\right) + \frac{1}{\gamma}\frac{\partial \hat{P}}{\partial \hat{y}} =$$

$$\epsilon Pr\left[2\frac{\partial^2 \hat{v}}{\partial \hat{y}^2} + \frac{\partial}{\partial \hat{x}}\left(\frac{\partial \hat{u}}{\partial \hat{y}} + \frac{\partial \hat{v}}{\partial \hat{x}}\right) - \frac{2}{3}\frac{\partial}{\partial \hat{y}}\left(\frac{\partial \hat{u}}{\partial \hat{x}} + \frac{\partial \hat{v}}{\partial \hat{y}}\right)\right],$$

heat,

$$\frac{1}{\gamma}\hat{\rho}\left(\frac{\partial\hat{T}}{\partial\hat{t}}+\hat{u}\frac{\partial\hat{T}}{\partial\hat{x}}+\hat{v}\frac{\partial\hat{T}}{\partial\hat{y}}\right)+\left(1-\frac{1}{\gamma}\right)\hat{P}\left(\frac{\partial\hat{u}}{\partial\hat{x}}+\frac{\partial\hat{v}}{\partial\hat{y}}\right)=$$

$$\epsilon\left(\frac{\partial^2\hat{T}}{\partial\hat{x}^2}+\frac{\partial^2\hat{T}}{\partial\hat{y}^2}\right)+(\gamma-1)\epsilon Pr\hat{\Phi}+(1-\sigma_p)\hat{W},$$

where

$$\hat{\Phi}=2\left(\frac{\partial\hat{u}}{\partial\hat{x}}\right)^2+2\left(\frac{\partial\hat{v}}{\partial\hat{y}}\right)^2+\left(\frac{\partial\hat{v}}{\partial\hat{x}}+\frac{\partial\hat{u}}{\partial\hat{y}}\right)^2-\frac{2}{3}\left(\frac{\partial\hat{u}}{\partial\hat{x}}+\frac{\partial\hat{v}}{\partial\hat{y}}\right)^2,$$

concentration,

$$\hat{\rho}\left(\frac{\partial\hat{C}}{\partial\hat{t}}+\hat{u}\frac{\partial\hat{C}}{\partial\hat{x}}+\hat{v}\frac{\partial\hat{C}}{\partial\hat{y}}\right)=\frac{\epsilon}{Le}\left(\frac{\partial^2\hat{C}}{\partial\hat{x}^2}+\frac{\partial^2\hat{C}}{\partial\hat{y}^2}\right)-\hat{W},$$

chemical kinetics,

$$\hat{W}=Z\hat{\rho}^2\hat{C}\exp\left(N_p(1-\hat{T}^{-1})\right)$$

To avoid too large a disparity between the spatio-temporal scales involved and the numerical complications this brings up, the numerical simulations are conducted for somewhat reduced value of the inverse Mach number a_p/u_p, compared to those typical of real-life explosives. Specifically, we set,

$$N_p = 4; \quad a_p/u_p = 10; \quad \sigma_p = 0.2; \quad Le = 1;$$

$$Pr = 1; \quad \gamma = 1.3; \quad \hat{l} = 0.25; \quad \hat{d} = 2, 10.$$

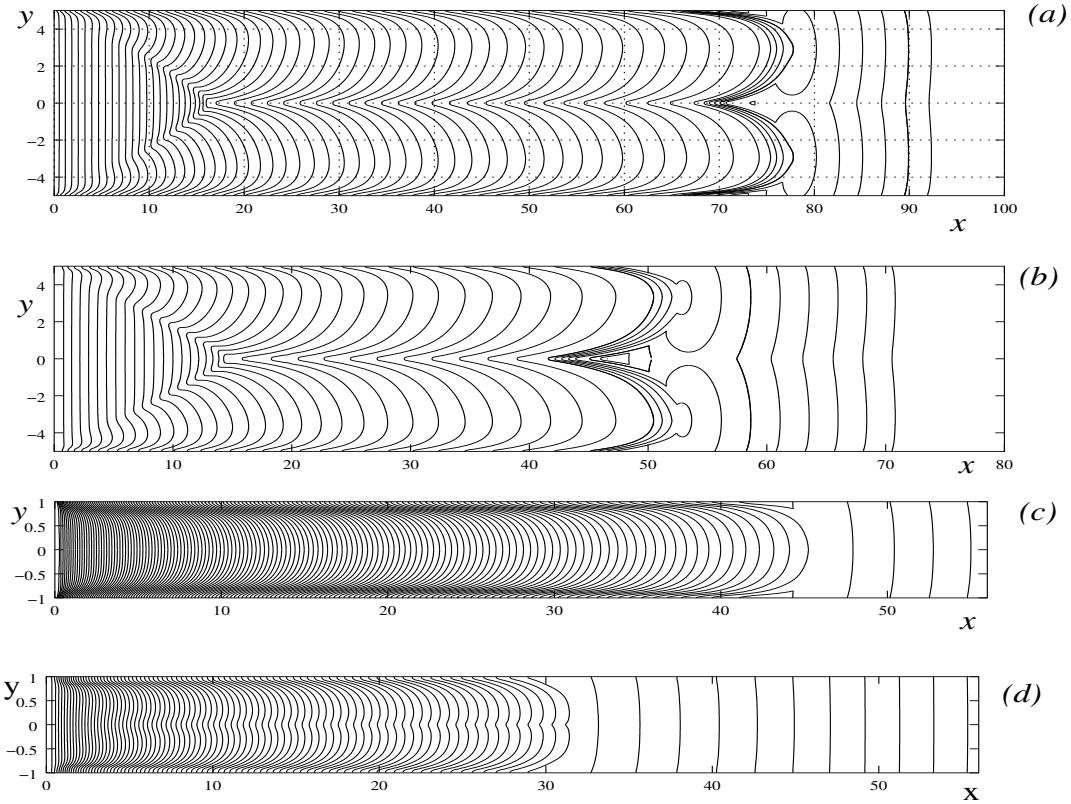

Figure 4: Temporal evolution of the reaction front. Scaled coordinates (x, y) are referred to 10 flame-widths. The parameters employed are specified as: $N = 4$, $Le = 1$, $Pr = 1$, $\epsilon = 0.01$, $\sigma = 0.2$, $\gamma = 1.3$, $d = 10$ $(a)(b)$ and $d = 2$ $(c)(d)$.Frames $(a)(c)$ - correspond to isothermal walls, and $(b)(d)$ to adiabatic walls. Frames $(c)(d)$ depict the reaction front profiles at several equidistant instants of the time.In the frames $(a)(b)$ the time intervals are equally spaced only up to the transition point, above which the intervals are subjected to the 5-fold reduction.

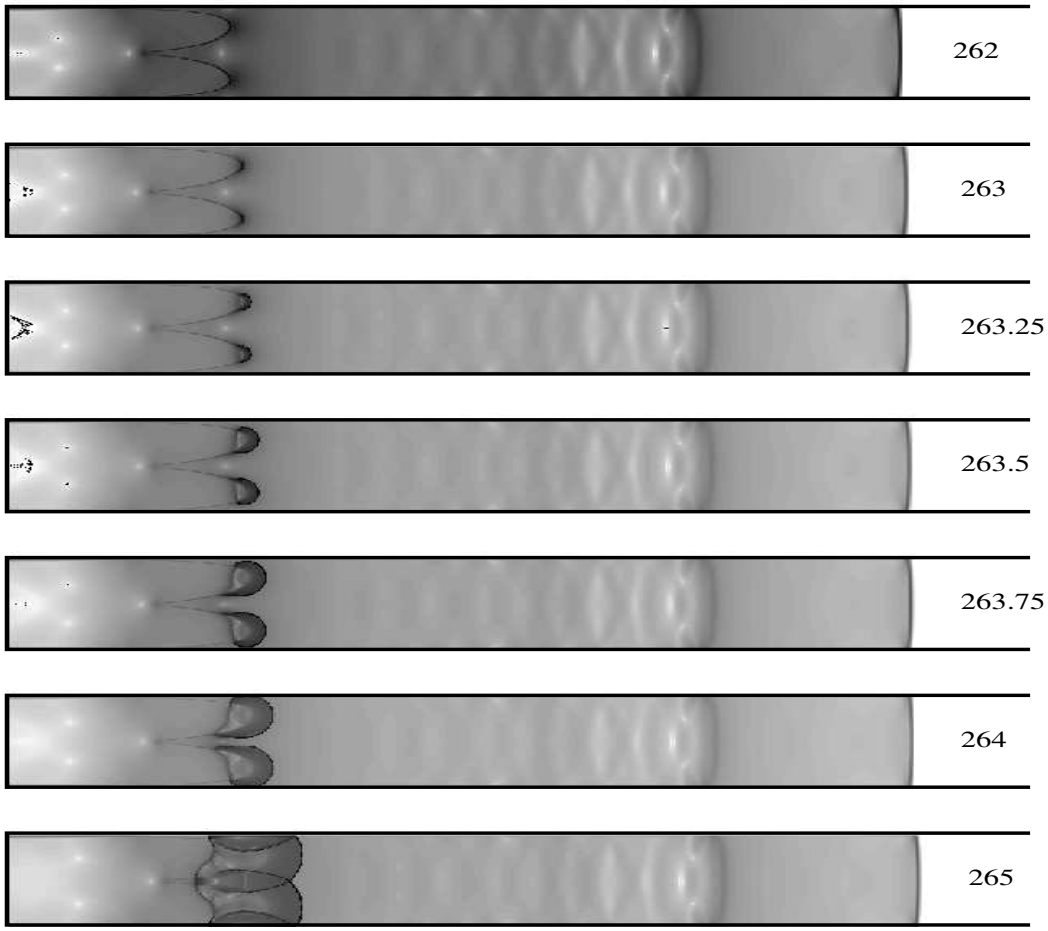

Figure 5: Pressure gradient norm at several consecutive instants of time (marked on the right). Stronger shading corresponds to higher pressure gradient. Parameters are identical to those of Fig. 1*a*.

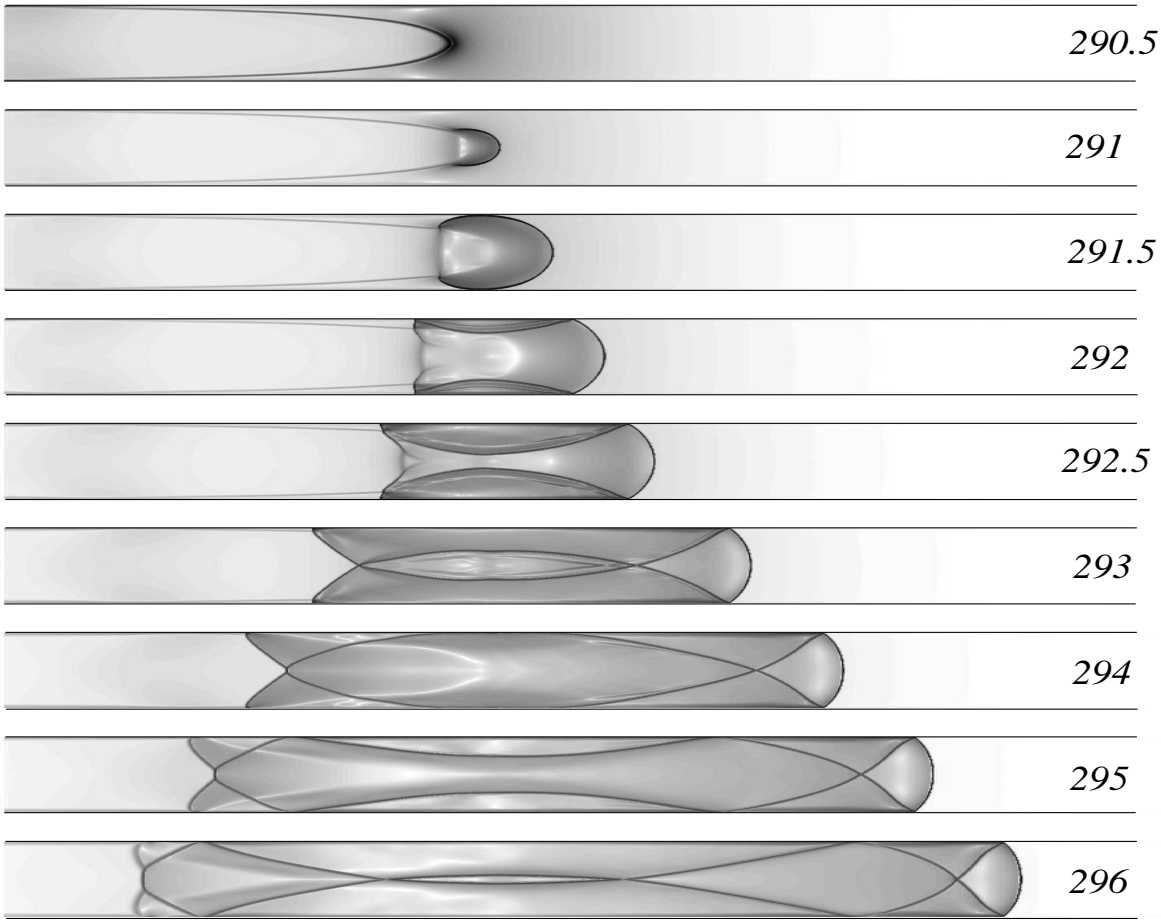

Figure 6: Pressure gradient norm at several consecutive instants of time (marked on the right). Stronger shading corresponds to higher pressure gradient. Parameters are identical to those of Fig. 1*c*.

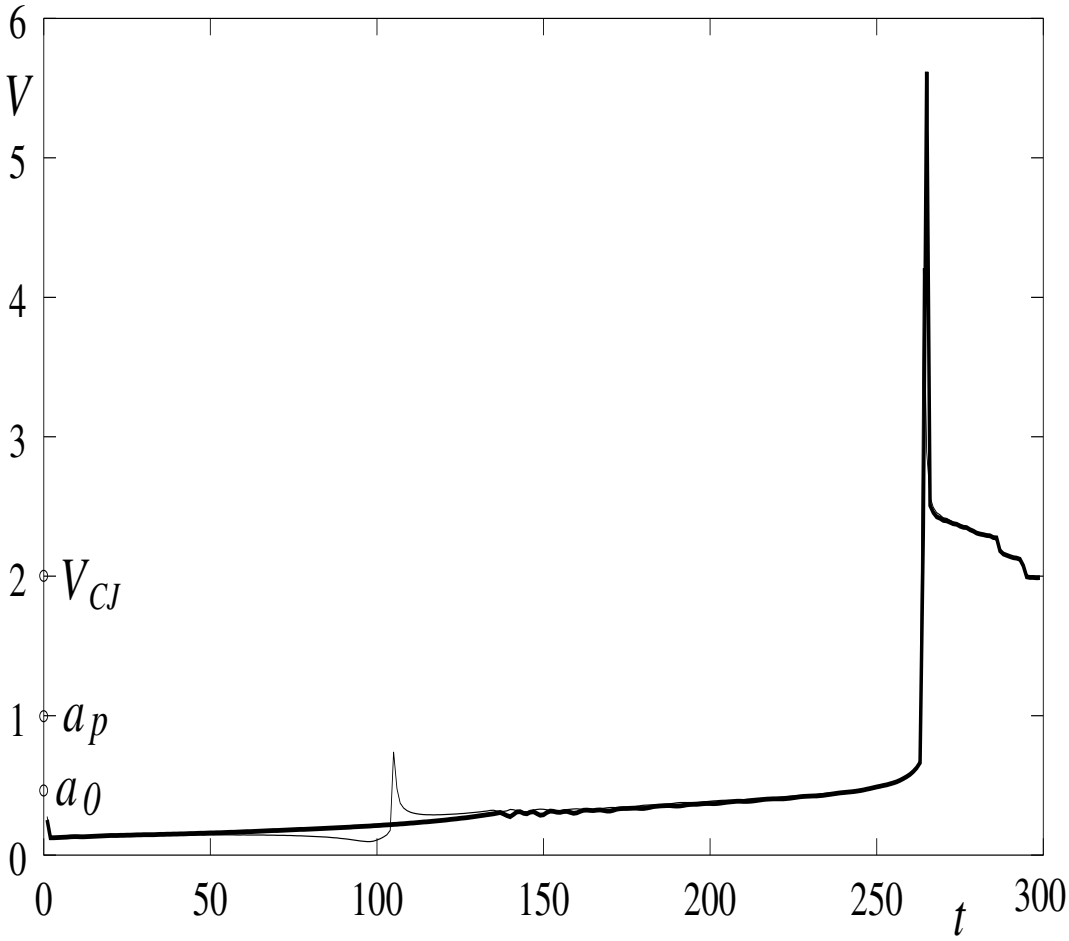

Figure 7: Reaction wave velocity V (scaled) versus time t (scaled). V_{CJ} corresponds to the Chapman-Jouget detonation; a_u, a_b - velocities of sound in the unburned and burned mixture, respectively. The bold/thin line correspond to $y = 4.5/1$, respectively. Parameters are identical to those of Fig. 1a

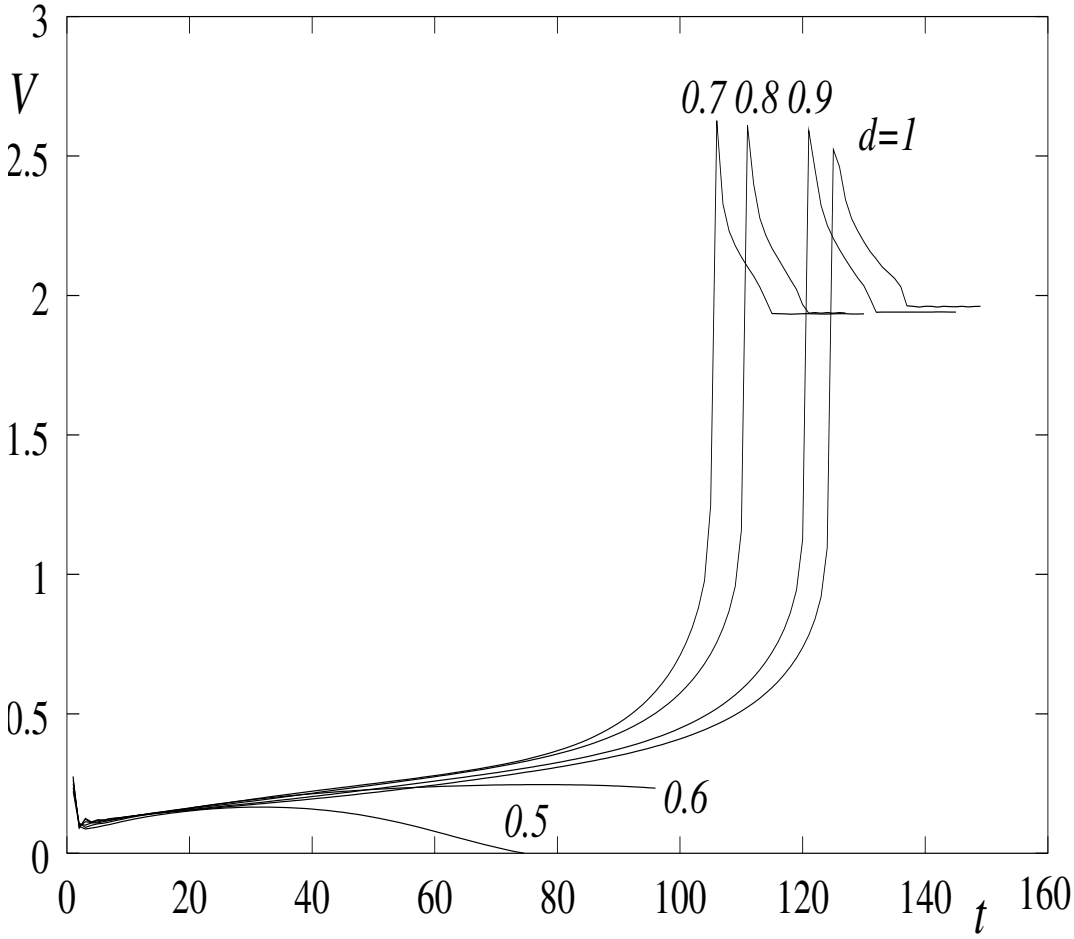

Figure 8: Reaction wave velocity V (scaled) versus time t (scaled) for several channel widths, d, at isothermal boundary conditions.